Navigation of Large Autonomously Controlled Formations

William A. Bamford*
Takuji Ebinuma†
E. Glenn Lightsey‡
The University of Texas at Austin, Austin, TX

In recent years, there has been substantial interest in autonomous satellite formations, driven by the new technologies that enable smaller and less costly spacecraft. Formation flying allows for certain mission designs, such as stereoscopic imaging, that are impractical or impossible using a single satellite. Much of the current work focuses on small formations, which can be defined as four or less satellites with a separation distance of a few kilometers. Next generation formations may be comprised of more satellites spanning greater spatial distances. The large formation problem becomes more difficult for several reasons, including an increased sensitivity towards modelling errors, and the effects of orbit perturbations, which become more important as the separation distance grows. The purpose of this work is to examine formation flying for large formations, and determine a dynamic and measurement model combination sufficient for accurate navigation. In order to lay the groundwork for large formation studies, a simulation environment is constructed which can handle varying separation distances. In order to draw numerical results from the research, a general formation is chosen, and Global Positioning System (GPS) receivers are used as the measurement sources. Different formation conditions are examined to determine the affect of separation on navigation accuracy

Introduction

The advantages of formation flying are numerous and can be applied to many different scientific fields. For example, a group of data gathering spacecraft could significantly improve the accuracy of space based interferometry by removing the physical hardware restrictions of a single satellite. Other missions, such as the Magnetospheric Multiscale Mission (MMS), will use a loosely constrained elliptical formation to simultaneously measure interactions of the magnetosphere from different positions in space.[1] The Terrestrial Planet Finder (TPF) will be able to directly detect and characterize Earth-like planets around other stars.[2] NASA lists several formation flying based missions in its flight plan.[3]

Many of the key developmental milestones, such as sensor development and formation control strategies, have been defined by Bauer.[4] Several potential formation types were categorized by Sabol.[5] Busse and How[6] demonstrated 1 cm position accuracy in a hardware simulation for a formation of spacecraft with a 1 km baseline using carrier phase differenced GPS measurements.

As the enabling technology matures, formation sizes may grow both in the number of participating satellites and in the inter-satellite distances. In anticipation of such missions, this research is designed as a first step towards the implementation of large baseline formations. A sample formation is simulated at various separation distances to determine the achievable level of positioning accuracy for the given dynamical model. An Extended Kalman Filter (EKF) is chosen for the on-board estimator. Double-differenced GPS signals are used as the measurement source, and are augmented, via an ionopspheric, model to correct for the growing importance of the ionosphere at larger separations.

The remainder of the paper is organized as follows. The next section lays out the basic estimator equations as well as the formation design. The construction of the filter models are then detailed. The results of simulations highlighting the performance of models and measurement schemes are presented for different separation distances. The final section discusses conclusions and the feasibility of controlling large formations such as the one presented here.

Background

The intent of this work is to determine the parameters required for the accurate relative position estimation of formations with large inter-satellite spacings. While the research is meant to be as general as possible, certain mission specifics must be selected to demonstrate basic principles and results. The example application is considered to be representative of a possible formation, but it is not suggested to be the only formation for which these performance trends are valid.

*Ph.D. Candidate, Department of Aerospace Engineering, The University of Texas at Austin.
†Research Fellow, University of Surrey
‡Assistant Professor, Department of Aerospace Engineering, The University of Texas at Austin.

Formation Control Architecture

The command hierarchy of autonomous formations have previously been categorized into three different architecture types: decentralized, centralized, and partially decentralized.[7] The centralized controller is characterized by a master satellite that receives measurements from each node and performs the state estimation for the formation. The node satellites may potentially require very little processing capability. The decentralized control architecture allows each individual node to process its own state locally. Some missions may necessitate the nodes to then share locally generated data, such as position vectors, for relative distance estimation. Since each spacecraft would need to possess the computational power to process its own state estimate, the decentralized controller may be more costly to implement. In a partially decentralized case, more than one node, but less than all the nodes, have the capability to process measurements and generate estimates. This concept reduces the single-point failure of the centralized case, while still allowing some nodes with minimal computational requirements.

For this study, a decentralized controller is chosen. While the filter algorithm is designed to accommodate several formation members, only two have been considered during filter validation. The satellites will share an orbit plane and utilize differences in their true anomalies to account for the inter-satellite separations. This configuration is illustrated in Figure 1. One satellite, which will be labelled the master satellite m will broadcast its GPS measurements to the other satellite, which will be designated as the node n. In this manner, the node will estimate a relative position vector with respect to the master. The performance of other architectures, as well as the inclusion of several more formation members will be considered in future work.

Filter Equations

Each node satellite will use an Extend Kalman Filter (EKF) for its state estimation. The estimation process can be represented with two phases, the time update phase and the measurement update phase. The EKF functions as a weighting scheme between the incoming measurements and the numerically computed system model.

System Model

The system model is composed of the equations of motion which will be used to represent the satellite's orbit, as well as the equations necessary to relate the incoming measurements to the satellite's state. The system model is characterized by:

$$\begin{aligned} \dot{\underline{x}}(t) &= F(\underline{x}(t), t) + \underline{w}(t) \\ \underline{y} &= G(\underline{x}(t)) + \underline{\nu}(t) \end{aligned} \tag{1}$$

where $\underline{x}$(t) is the true state vector and $\underline{y}$ is the measurement set. Each measurement set has noise, $\underline{\nu}(t)$, associated with it, and $\underline{w}$(t) is the noise attributed to the system model. These noise terms have the properties:

$$\begin{aligned} E|\underline{w}(t)\underline{w}^T(\tau)| &= Q(t)\delta(t-\tau) \\ E|\underline{\nu}(t)\underline{\nu}^T(\tau)| &= R(t)\delta(t-\tau) \end{aligned} \tag{2}$$

Q(t) is known as the dynamic model covariance, and *R(t)* is the measurement model covariance. Both of these matrices can be used as tuning parameters for the filter.

Propagation Equations

Between measurements, the state and state covariance must be propagated forward in time. If we designate the (-) as values prior to the measurement being received at time k, and (+) corresponding to the values after the update, the propagation equations have the form:

$$\begin{aligned} P_{k+1}(-) &= \Phi(t_{k+1}, t_k) P_k(+) \Phi^T(t_{k+1}, t_k) + Q_{k+1} \\ A_k &= \frac{\partial F}{\partial \underline{x}}|_{\underline{x}=\hat{\underline{x}}_k(-)} \\ \dot{\Phi}(t, t_{k-1}) &= A(t)\Phi(t, t_{k-1}) \end{aligned}$$

with the initial matrix

$$\Phi(t_{k-1}, t_{k-1}) = I$$

where $\Phi(t, t_{k-1})$ is the state transition matrix which is used to propagate the covariance matrix P from time t_{k-1} to time t_k. The $\hat{}$ symbol indicates that the vector is an estimated quantity.

Update Equations

Once a measurement is introduced the filter can use it, in conjunction with the system model, to estimate an updated position and covariance.

$$\begin{aligned} \hat{\underline{y}}_k &= G(\hat{\underline{x}}_k(-), t_k) \\ \underline{z}_k &= \underline{y}_k - \hat{\underline{y}}_k \\ H_k &= \frac{\partial G}{\partial \underline{x}}|_{\underline{x}=\hat{\underline{x}}_k(-)} \end{aligned}$$

where $\underline{y}_k$ is the actual measurement, $\underline{z}_k$ is the measurement residual, and $\hat{\underline{y}}_k$ is the measurement computed from the measurement model. The state and the covariance matrix are updated using:

$$\begin{aligned} P_k(+) &= (I - K_k H_k) P_k(-) (I - K_k H_k)^T + K_k R_k K_k^T \\ \hat{\underline{x}}_k(+) &= \hat{\underline{x}}_k(-) + K_k \underline{z}_k \\ K_k &= P_k(-) H_k^T [H_k P_k(-) H_k^T + R_k]^{-1} \end{aligned} \tag{3}$$

with I being the appropriately sized identity matrix, and K being the Kalman gain.

Filter Design

The EKF design process requires the definition of the state, determination of the measurement and dynamic models, and linearization of these models for the

measurement update and the state transition update respectively. The filter must then be started by providing it with initial state estimates $\hat{x}_0(-)$, the measurement noise covariance R_0, and the process noise covariance Q_0.

GPS Measurements

Following the notation given by Ebinuma,[10] the GPS measurements, pseudorange p, carrier-phase ϕ, and range-rate d received at any receiver, can be modelled by:

$$p(t) = \rho(t) + c(\delta t - \delta t_{GPS}) + I + \epsilon_P \quad (4)$$

$$\phi(t) = \rho(t) + c(\delta t - \delta t_{GPS}) - I + \lambda n + \epsilon_\Phi \quad (5)$$

$$d(t) = \dot{\rho} + c(\delta f - \delta f_{GPS}) - \dot{I} + \epsilon_D \quad (6)$$

where δt and δt_{GPS} are the receiver's clock offset and the GPS satellite's clock offset respectively, and the δf terms represent the frequency offsets. The I term represents the ionospheric path delay, and the ϵ terms encompass all other unmodeled errors, including electrical noise and multipath. At the time of transmission $(t-\tau)$ the true range between a GPS satellite and thereceiver can be expressed as:

$$\rho(t) = |\underline{r}(t) - \underline{r}_{GPS}(t-\tau)| \quad (7)$$

The associated range-rate is found from

$$\dot{\rho} = \underline{e}^T(\dot{\underline{r}} - \dot{\underline{r}}_{GPS}(t-\tau)) \quad (8)$$

here, $\underline{e}$ is the line of sight vector between the satellite and the receiver, and is given by:

$$\underline{e}(t) = \frac{\underline{r}(t) - \underline{r}_{GPS}(t-\tau)}{\rho(t)} \quad (9)$$

The λn term in Equation 5 represents the integer carrier cycle ambiguity. While the GPS receiver is capable of determining which portion of the carrier wave it is receiving, it is unable to detect how many integer wavelengths exist between itself and the GPS satellite. To utilize the carrier phase as a measurement source, this integer must be resolved for each satellite being tracked.

By subtracting measurements made by both receivers from a pair of common-view GPS satellites, known as a double difference, errors such as the GPS satellite clock offset and receiver clock offset are removed. The relative position vector between the master and node satellite can be written as:

$$\underline{r}_m = \underline{r}_n + \Delta\underline{r} \quad (10)$$

as depicted in Figure 1. Performing a double-difference to Equations 4-6 from common GPS satellites A and B yields:

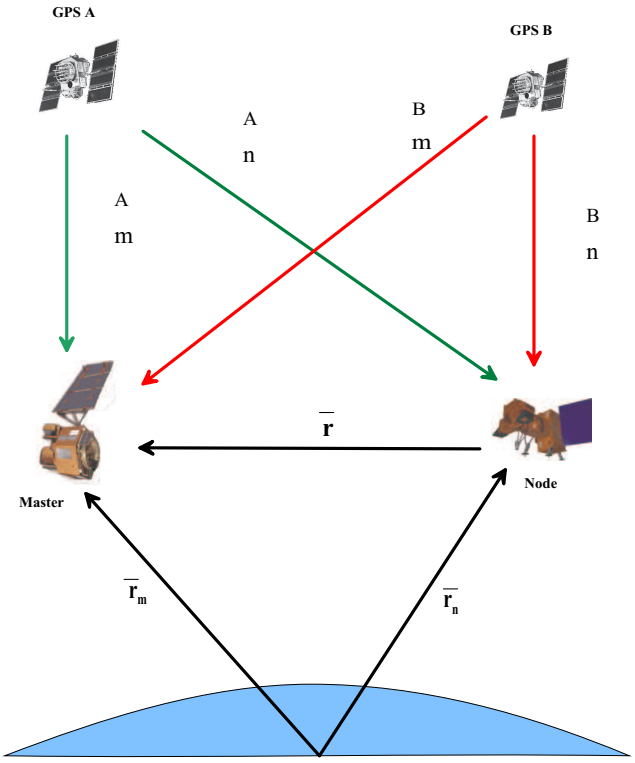

Fig. 1 Relative Vector Diagram

$$\begin{aligned}
\Delta\delta p^{AB}(t) &= \{|\underline{r}_n(t) + \Delta\underline{r} - \underline{r}^A_{GPS}(t-\tau)| - \\
&\quad |\underline{r}_n(t) - \underline{r}^A_{GPS}(t-\tau)|\} - \{|\underline{r}_n(t) + \Delta\underline{r} - \\
&\quad \underline{r}^B_{GPS}(t-\tau)| - |\underline{r}_n(t) - \underline{r}^B_{GPS}(t-\tau)|\} + \\
&\quad \Delta\delta I + \Delta\delta\epsilon_p \\
\Delta\delta\phi^{AB}(t) &= \{|\underline{r}_n(t) + \Delta\underline{r} - \underline{r}^A_{GPS}(t-\tau)| - \\
&\quad |\underline{r}_f(t) - \underline{r}^A_{GPS}(t-\tau)|\} - \\
&\quad \{|\underline{r}_n(t) + \Delta\underline{r} - \underline{r}^B_{GPS}(t-\tau)| - |\underline{r}_f(t) - \\
&\quad \underline{r}^B_{GPS}(t-\tau)|\} - \Delta\delta I + \lambda\Delta\delta n + \Delta\delta\epsilon_\phi \\
\Delta d^{AB}(t) &= \{\underline{e}^T\Delta\dot{\underline{r}}_n(t) + \Delta\underline{e}^T(\dot{\underline{r}}_n(t) - \\
&\quad \dot{\underline{r}}^A_{GPS}(t-\tau))\} - \{\underline{e}^T\Delta\dot{\underline{r}}_n(t) + \\
&\quad \Delta\underline{e}^T(\dot{\underline{r}}_n(t) - \dot{\underline{r}}^B_{GPS}(t-\tau))\} - \Delta\delta\dot{I} + \Delta\delta\epsilon_d
\end{aligned} \quad (11)$$

The $\Delta\delta$ notation signifies a double-difference is to be performed.

State Definition

The state vector at time k is defined as

$$\underline{x}_k = [\Delta\underline{r} \quad \Delta\dot{\underline{r}} \quad \Delta\delta n_1 \quad \ldots \quad \Delta\delta n_j]^T \quad (12)$$

where $\Delta\underline{r}$ is the relative distance and $\Delta\dot{\underline{r}}$ is the relative velocity of the node with respect to the master. $\Delta\delta n$ is the double-differenced integer ambiguity for the j satellites tracked by both of the formation members.

Dynamic Model

As the inter-satellite spacing increases, the dynamic model becomes increasingly sensitive to orbit perturbations. For smaller baseline formations, a linearized

approach such as Hill's Equations may be adequate as the plant model. Since the basic assumptions of Hill's equations break down as the separation increases, a numerically integrated plant model is chosen. For simplicity, the model in this study is limited to the two-body equations of motion augmented by drag and J2 perturbations:

$$\ddot{x} = \frac{-\mu x}{r^3}(1 - \frac{3}{2}J_2(\frac{r_e}{r})^2(5\frac{z^2}{r^2} - 1)) - \frac{1}{2}C_D\frac{A}{m}\rho v(\dot{x} - \omega_E y)$$
$$\ddot{y} = \frac{-\mu y}{r^3}(1 - \frac{3}{2}J_2(\frac{r_e}{r})^2(5\frac{z^2}{r^2} - 1)) - \frac{1}{2}C_D\frac{A}{m}\rho v(\dot{y} + \omega_E x)$$
$$\ddot{z} = \frac{-\mu z}{r^3}(1 - \frac{3}{2}J_2(\frac{r_e}{r})^2(5\frac{z^2}{r^2} - 3)) - \frac{1}{2}C_D\frac{A}{m}\rho v\dot{z}$$

where r_E is the radius of the Earth, ω_E is its rotation rate and μ is the Earth's gravitational parameter. C_D is the satellite's drag coefficient, A is its cross-sectional area, and m is the mass of the satellite. ρ is the atmospheric density, which is found via an exponential model, and v is the relative wind, given by

$$v = |\frac{d\underline{r}}{dt} - \underline{\omega}_E \times \underline{r}| \tag{13}$$

Measurement Model

The measurement model is based on the double-differenced carrier phase and doppler measurements between the leading and trailing satellites. The measurement vector is represented as:

$$\underline{y} = [\Delta\underline{\phi} \quad \Delta\underline{d}]^T \tag{14}$$

where $\Delta\underline{\phi}$ and $\Delta\underline{d}$ are vectors, each containing j differenced measurements. The differential measurements can be modelled by the non-linear equations given in equation 11. The ionospheric path delay is modelled by:

$$\Phi_{delay} = \frac{82.1*TEC}{F_c^2*\sqrt{sin^2(EL)+0.076}+sin(EL)} \tag{15}$$

where Φ_{delay} is the delay of the carrier phase measurement in meters, EL is the elevation of the GPS satellite with respect to the receiver's local horizon, and TEC is the total number of electrons between the receiver and the GPS satellite.

The GPS satellite states can be determined from their broadcast ephemeredes, and the measurement vector length is dependent upon the number of GPS satellites tracked at the given epoch.

Simulation and Results

The simulation environment and filtering code were originally developed in Matlab. To verify the numerical simulation, a Spirent STR4760 GPS signal simulator was used to provide measurements to two Orion GPS receivers. The initial orbital elements were provided to the simulator, which then propagated them forward using a 10x10 gravity model with the desired

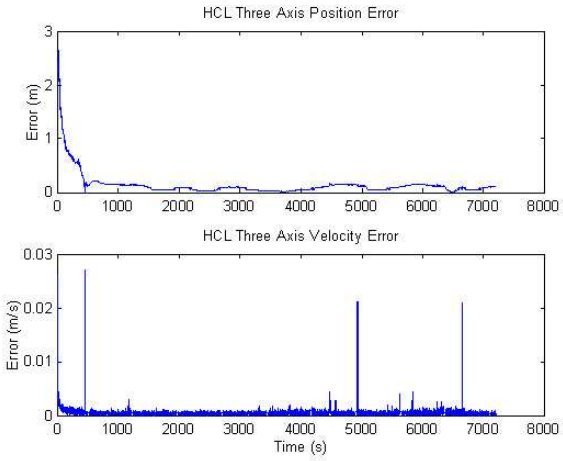

Fig. 2 HCL Error for 1km Separation

perturbations. The spacecraft were modelled as identical symmetric spacecraft with a surface area of 2 m^2, a Cd of 2, and mass of 100 kg. A simple ionospheric model, which consisted of a constant electron count augmented by a sinusoidal variation, was also implemented. Multi-path error is not accounted for in this study, but could be investigated in future studies.

Filter Initialization

Each of the filter states must be initialized at the beginning of the simulation, and the double-differenced ambiguity parameters must be re-initialized every time a new satellite combination is simultaneously tracked by both receivers. The leading satellite is initialized in a circular orbit with an altitude of 445 km and an 87 degree inclination. The trailing satellite adopts the same orbit plane but is rotated backwards in true anomaly until the desired separation distance is obtained.

Each of the double-differenced integer ambiguities can be initialized using the carrier-phase and pseudo-range measurements from common GPS satellites A and B:

$$\Delta\delta N = \{(p_m^A - \phi_m^A) - (p_n^A - \phi_n^A)\} - \{(p_m^B - \phi_m^B) - (p_n^B - \phi_n^B)\} \tag{16}$$

Results

Figure 2 illustrates the results from the 1 kilometer separation case. The accuracy of the filter agrees closely to published works for similar formations.

It is interesting to note that the accuracy was very similar with no ionospheric path delay modelled. As the formation separation was increased to 100 km, the effect of the ionospheric becomes more pronounced in the relative estimation. Figure 3 depicts the double-differenced path delay for one pair of GPS satellites. This error is significant enough to cause problems in ambiguity resolution if not accounted for in the measurement model. The estimation errors and for the 100

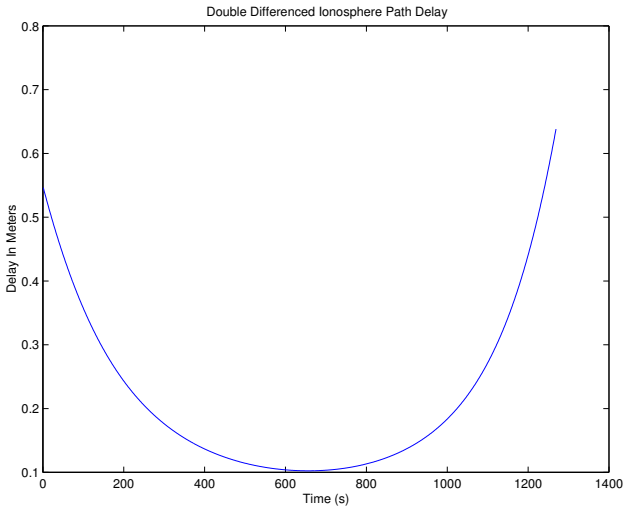

Fig. 3 Ionospheric Path Delay for 100km Separation

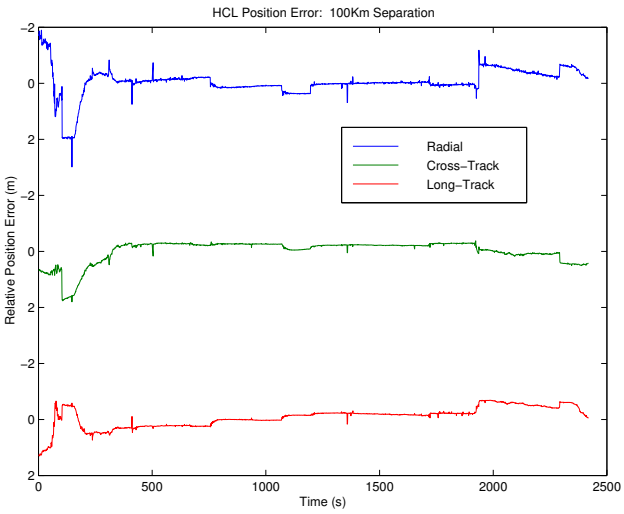

Fig. 4 HCL Error for 100km Separation

Table 1 Relative Position Error Summary (meters)

	Radial	Cross Track	Along Track
1km	0.04 ± 0.03	0.05 ± 0.03	0.03 ± 0.00
100km	-0.01 ± 0.07	0.11 ± 0.03	0.02 ± 0.09
500km	-0.20 ± 0.11	0.27 ± 0.08	-0.02 ± 0.05

km separation formation are plotted in Figure 4. Since the node's absolute position is provided via the GPS position fix solution, the relative accuracy is, to some extent, sensitive to discontinuities in the receiver's solution.

The small spikes in the error plots occur in tandem to spikes in the receiver's absolute position. The large biases stem from the filter's slow response to jumps in the absolute position estimation. The 10 cm accuracies demonstrated for the 100 km baseline case were developed with a minimal amount of tuning. A more rigorous tuning may provide even better results.
The 500km scenario has been included for completeness, and work is ongoing to better model this case. Once the ambiguities are correctly estimated, the relative position solutions behave as expected. However, as illustrated in Figure 5, it takes nearly 12 minutes for the filter to correctly determine these parameters. The jumps in the absolute position skew the ambiguity parameters causing delayed convergence, and resulting in 20cm biases in the solutions. Table 1 summarizes the filter's performance for these three formations. The accuracies reported for the 500km are computed only after the ambiguities have been resolved, making these numbers optimistic.

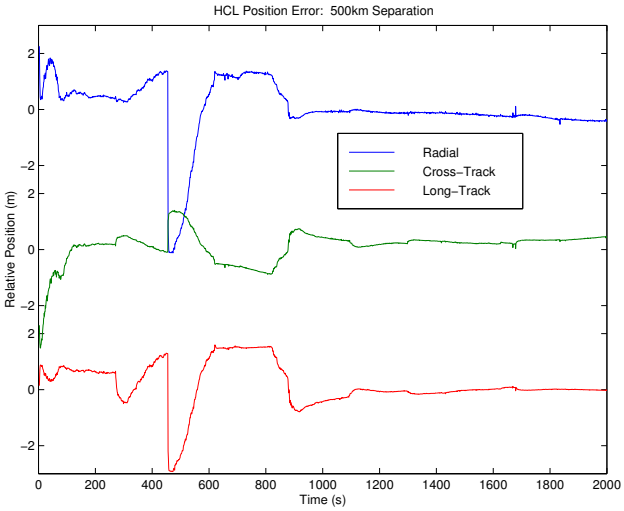

Fig. 5 HCL Error for 500km Separation

Conclusions

The controller architecture and formation design chosen for this study were chosen for their scalability. An Extended Kalman Filter was developed which could handle formations with small and large inter-satellite separations. The filter was validated by comparing its estimation errors to other published works for a 1 km separation. The same filter was then used for relative state vector estimation at the 100 and 500km separations. It was demonstrated that even at 100km, relative position accuracy of 10cm can be achieved. The main flaw in the current filter design is its inability to handle some of the larger jumps in the absolute position fix solution. This condition was most evident in the 500km scenario. Future work will focus on minimizing or removing this problem, as well as implementing a more realistic ionospheric model in the simulated environment. The final step will be to incorporate this code into the real-time GPS simulation environment at the University of Texas' Center for Space Research.

Acknowledgements

The author would like to thank Goddard Space Flight Center, whose grants have made this research possible.

References

[1]http://stp.gsfc.nasa.gov/missions/mms/mms.htm.

[2]http://planetquest.jpl.nasa.gov/TPF/tpf index.html.

[3]http://gsfctechnology.gsfc.nasa.gov/dssmissionlist.htm.

[4]F. Bauer, K. Hartman, J. How, J. Bristow, D. Weidow, F. Busse, "Enabling Spacecraft Formation Flying through Spaceborn GPS and Enhanced Autonomy Technologies," September 1999.

[5]C. Sabol, R. Burns, C. McLaughlin, "Satellite Formation Flying Design and Evolution," *Spaceflight Mechanics*, edited by Bishop, Vol. 102, American Astronautical Society, February 1999, pp. 265–284.

[6]Busse, F. and How, J., "Real-Time Experimental Demonstration of Precise Decentralized Relative Navigation For Formation Flying Spacecraft," *Proc. of the AIAA Guidance, Navigation, and Control Conference and Exhibit*, August 2002, Monterey, CA.

[7]Carpenter, J., "Partially Decentralized Control Architectures for Satellite Formations," *Proc. of AIAA GNC Conference*, Monterey, August 2002.

[8]Vallado, D., *Fundamentals of Astrodynamics and Applications*, McGraw Hill, 1997.

[9]E.M.C. Kong, D.W. Miller, R.J. Sedwick, "Exploiting Orbital Dynamics for Aperture Synthesis Using Distributed Satellite Systems: Applications to a Visible Earth Imager System," *Spacefight Mechanics 1999*, edited by Bishop, Vol. 102, American Astronautical Society, February 1999, pp. 285–301.

[10]T. Ebinuma, O. Montenbruck, E.G. Lightsey, "Precise Spacecraft Relative Navigation Using Kinematic Inter-Spacecraft State Estimtes," *ION GPS-2002*, Portland, Oregon, September 2002.

[11]Ebinuma, T., *Precision Spacecraft Rendevous Using the Global Positioning System: An Integrated Approach*, Ph.D. thesis, University of Texas at Austin, 2000.